Water cooled turbocharger heat transfer model initialization: Turbine and compressor quasi-adiabatic maps generation

Georges Salameh, Guillaume Goumy, Pascal Chesse

Water cooled turbocharger heat transfer model initialization: turbine and compressor quasi-adiabatic maps generation

Georges SALAMEH (corresponding author)
Ecole Centrale de Nantes
1 rue de la Noë, 44321 Nantes cedex 3 – France
georges.salameh@ec-nantes.fr

Guillaume GOUMY
Ecole Centrale de Nantes
1 rue de la Noë, 44321 Nantes cedex 3 – France
guillaume.goumy@ec-nantes.fr

Pascal CHESSE
Ecole Centrale de Nantes
1 rue de la Noë, 44321 Nantes cedex 3 – France
pascal.chesse@ec-nantes.fr

ABSTRACT

Water cooled turbochargers used in gasoline engines present a difficulty in studies due to heat transfers in both the turbine and the compressor. Data available for users is usually measured in stable operating conditions with high temperature gradients on the turbine side which affects the compressor and the whole turbocharger. The heat transfers between the different elements are not quantified. Heat transfer models are necessary to quantify the amount of heat exchanged with an element and calculate then the real amount of work produced or consumed. A lumped mass heat transfer model is presented in this paper where every element of the turbocharger is considered as a thermal mass. Three main elements are represented: the turbine, the compressor and the central housing. The heat transfer model is then used to generate compressor and turbine quasi-adiabatic maps using supplier maps and geometrical data without more complicated tests. An experimental campaign is conducted to validate the model and show the effect of the water cooling on the thermal transfer between the turbocharger elements. In this model, the compressor and the turbine are treated separately and the water cooling is considered as a thermal barrier between the two. No coupling between the compressor and the turbine heat transfer models is needed which simplifies the calculation compared to other models.

KEYWORDS:

Turbocharging; centrifugal compressor; radial turbine; heat transfer; water cooling; adiabatic.

1 Introduction

With emissions and fuel consumption norms and regulations becoming more and more strict, turbocharging is widespread in automotive field. In Diesel engines, turbocharging is a primary technique to supply the engine intake with compressed air. It is used also in gasoline engines mainly for downsizing that is seen as a solution for the new regulations. This technology requires many modifications and developments carried out with studies and tests. There are the waste gate or the variable geometry turbine turbochargers or even two-stage turbochargers for new engines with high efficiency. The use of electrical driven compressors or e-boost components is spreading in new engine development to avoid the problems from the turbine-compressor interaction [1].

Turbochargers need to be modeled by automotive manufacturers in commercial software for internal combustion engine simulations. They can be used for engine calibration, ECU, HIL, or to test new architectures. Numerical models did not evolve at the same speed as the technology implemented. They are based on performance maps for the turbine and the compressor, usually given by the supplier. These supplier performance maps are measured at high temperatures. At such high temperatures, thermal transfers must be considered as an important phenomenon among others. The main effect of the thermal transfers is on the calculation of the efficiencies. The turbine and compressor efficiencies are calculated using measured temperatures and pressures and assuming a steady state flow of an ideal gas with a constant specific heat in an adiabatic process. The thermal gradient can be about hundreds of degrees between the exhaust gases on the turbine side and the intake gases on the compressor side. The effect of the

58 thermal transfers for predicting engine performance is presented by Serrano et al. [2].
59 Their effect on the compressor efficiency is increased at lower rotational speeds as
60 pointed out by Chesse et al. [3].

61 Heat transfer models used in internal combustion engines can be more or less
62 complicated: they can go from three dimensional models to lump masses models. A
63 model is not complex only because of the calculation time and power, but also because of
64 the data required. This data is not always available for the users. A simple model with the
65 minimum complexity and available data is then essential for the turbocharger heat
66 transfer calculation. In the works of Bohn et al. [4], a three dimensional model quantifies
67 and predicts the heat transfers for different operating points using a Nusselt correlation
68 and shows their effect between the high temperature side turbine and the low
69 temperatures side compressor. A one dimensional lump mass model is developed by
70 Olmeda et al. [5] where the whole turbocharger is split into different metal nodes. The
71 heat transfers are calculated between every metal element and its adjacent, and between
72 the metal and the fluid. The works of Romagnoli et al. [6] present a lump mass model to
73 evaluate the heat transfer in the turbine; it shows that the surface temperature of the
74 compressor and the turbine vary linearly with the exhaust gases temperature and that the
75 temperature of the bearing housing varies consistently with the oil temperature. A lump
76 mass model is presented by Serrano et al. [7] where the turbocharger is divided into five
77 lump masses: the heat transfer is calculated between the different parts, and between
78 these parts and the ambient air. Many parameters are needed in this model and their
79 calibration requires specific tests that are not always available for users. This also makes
80 this model more difficult to apply on different turbochargers. A simpler version of the

model of Serrano et al. [8] is presented to allow creating turbine and compressor adiabatic performance maps using the supplier performance maps. The calculation is done on every operating point of the turbine and the compressor iteratively to find out the outlet temperature. Hypothesis are used to evaluate the pressure ratio and the efficiency of the other part of the turbocharger since it is not possible to find the operating point of the turbine on the turbine map and its corresponding operating point on the compressor map.

To evaluate the heat transfers in turbochargers experimentally, there are different studies. The surface temperature measurement with an infrared camera can be done as in the works of Tanda et al. [9]. The temperature gradient can be evaluated along the turbocharger and the conduction heat transfer can be calculated. Empirical correlations are presented: the first one links the heat transfer to the difference between the oil temperature and the compressor inlet air temperature; the second one uses the central housing and the compressor wall temperatures. The results are satisfactory but the calibration process requires a specific measurement that is not available for all users. Experimental measurements are presented by Baines et al. [10] where different turbochargers are tested with different bearing systems. The environment conditions element are also studied to see their effect on the turbocharger performance. The turbine inlet temperature has an important impact on the turbine performance, and the compressor efficiency depends on the turbine and the oil inlet temperatures. The heat transfers in the turbocharger need to be studied in a global aspect taking into account all the elements. On the turbine side, heat transfers occur mainly before the impeller and in the experimental data of Baines et al. [10], the main heat transfer from the turbine is

103 estimated with the environment, and a lower part with the oil and a small remaining
104 amount with the compressor.

105 The compressor heat transfer model presented by Marelli et al. [11] is used to
106 transform the supplier compressor performance map into a quasi-adiabatic map. This
107 model is applied on the compressor only and depends a lot on the oil and water
108 temperatures. This model requires geometrical data not always available for the user.
109 Serrano et al. [12] also developed an internal convection heat transfer model applied on a
110 cooled turbocharger; it shows the effect of the oil and coolant temperature on the thermal
111 transfers. These heat transfers are considered mainly at the turbine inlet and the
112 compressor outlet. The effect of the heat transfer on the performance of a turbocharger is
113 presented in the works of Sirakov and Casey [13]. A method to transform a turbocharger
114 supplier map into an adiabatic map is detailed. The particularity of this method is the
115 assumption of a constant heat flow for the turbocharger operating points. This hypothesis
116 can be rough: the heat flow should be considered variable with the operating points. Savic
117 et al. [14] quantifie the heat transfers in the turbocharger using the power calculation. The
118 comparison between the supplier conditions and the adiabatic data becomes simpler but
119 this approach requires knowing the turbine and compressor effective power for every
120 operating point which is not the case when using SAE supplier maps. The model of Gao
121 et al. [15] is also based on a three dimensional conjugate heat transfer simulation to
122 quantify the external heat transfers on the turbine side: it is noticed that the greatest part
123 of the internal heat transfer in the turbine occurs in the volute. In the approach of Casey et
124 al. [16], the heat transfer effect is implemented into the calculation with a polytropic
125 transformation assumption instead of an isentropic. There is no need to add a heat transfer

model since it is calculated directly in the transformation model but it requires important changes like the supplier maps that need to be calculated using the new approach.

The effect of heat transfer on water cooled turbocharger performance is tested in the works of Cormerais et al. [17] and Marelli et al. [18][19]. The water cooling has an important impact on the turbocharger components mass flow rates and efficiencies. Water cooling reduces the heat transfers between the turbine and the compressor and it could be considered as a thermal barrier. A more detailed calculation on Gasoline engine turbochargers heat transfers is presented by Jiaqiang et al. [20] where a CFD calculation shows the influence of the water boiling heat transfer on the thermal transfers in the turbocharger, the void fraction and the temperature field in the water section.

A three masses lumped model is presented by Sanguinetti et al. [21] where the heat transfer is quantified in every element between the body of this element and the fluid going inside, the surrounding environment, and the adjacent element or elements. Goumy et al. [22] continued the work on this model and presented a method to calculate quasi-adiabatic maps from supplier maps using the heat transfer model. This paper presents the continuation of the model of Goumy et al. [22] on water cooled turbochargers. The difference presented in this paper is the separation of the turbine and the compressor heat transfer models. The heat transfer is calculated in the turbine and the compressor separately since the water cooling is considered as a thermal barrier between the two. This method could be very useful for automotive manufacturers when using engine simulation with a turbocharger model based on the supplier maps. In the first part, experimental measurements are presented to show the supplier and adiabatic conditions. The heat transfer model is presented with the validation of the thermal barrier concept,

149 the friction model used and the central housing constant temperature calculation. In the
150 last part, adiabatic turbine and compressor performance maps are generated using
151 supplier maps and applying the heat transfer model.

152 **2 Experimental measurements:**

153 The experimental tests are carried on a turbocharger test bench at Centrale Nantes
154 with modifications according to each turbocharger specifications. The main diagram of
155 the test bench is shown in Fig. 1. The detailed presentation of the test bench can be found
156 in the works of Salameh et al. [23][24]. The turbine is fed with compressed air coming
157 from a screw compressor, a filter, a dryer, a pressure regulator and an electric heater to
158 regulate the turbine inlet temperature. An electric valve is used to regulate the turbine
159 mass flow rate and expansion ratio. The air is extracted at the turbine outlet using an
160 extractor fan.

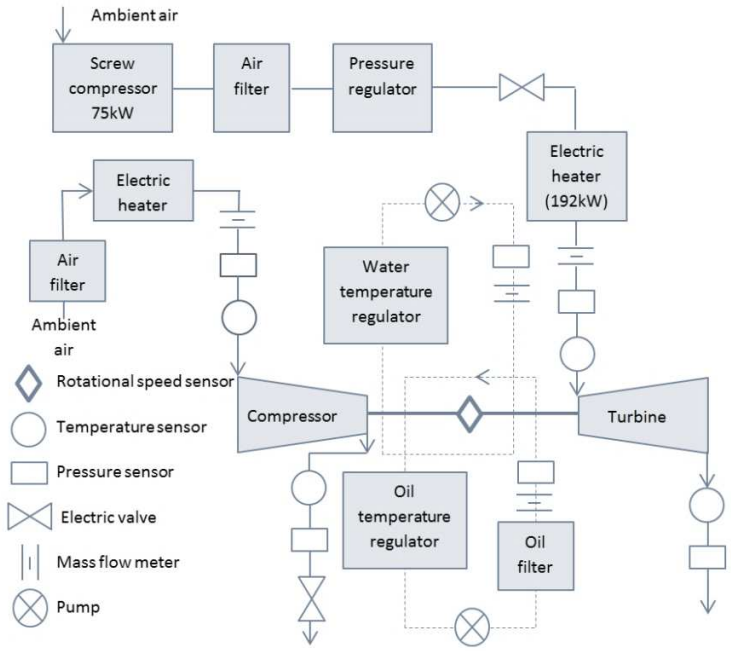

Fig. 1. Turbocharger test bench

On the compressor side, ambient air is filtered and then goes through a mass flow rate sensor and into the compressor inlet. An electric valve at the compressor outlet controls the pressure at the compressor outlet and hereby the compressor mass flow rate and the turbocharger rotational speed. The compressor exhaust is rejected to the outside with an extractor fan. Pressure and temperature sensors are installed at the compressor inlet and outlet.

Sensor	**Type**	**Range**	**Precision**
Temperature	Type T	-185 – 300 °C	± 0.1°C
	Type N	0 – 1185 °C	± 0.1°C
		0 – 100 mbar	±1.5 mbar
		0 – 350 mbar	±5.25 mbar

Pressure	Air: First sensor HMA	0 – 2500 mbar	±30 mbar
		0 – 5000 mbar	±75 mbar
	Atmospheric pressure: first sensor HMA BARO	800 – 1100 mbar	±10 mbar
	Oil pressure : First sensor CTU	0 – 5000 mbar	±0.02% per °C (from -20°C)
Rotor regime sensor	Picoturn inductive sensor	0 – 300 000 rpm	± 200 rpm
Mass flow rate	Air: Krohne optiswirl	50 – 550 $kg.h^{-1}$	±1.5%
	Oil : Bamo micro stream	0.5 – 50 $l.h^{-1}$	±2%

169 **Table 1.** Characteristics and precision of the sensors used in the experimental study

170 Two types of temperature sensors are used according to the measured values. The
171 pressure sensors are different according to the measurement range. The central housing is
172 equipped with sensors for the lubricating oil and the cooling water. The oil inlet pressure
173 and temperature are regulated using a pump and a heater, and so are the water inlet
174 conditions. The different sensors specifications and precision are presented in Table 1.

175 The turbocharger presented in this study is a small gasoline engine water-cooled
176 turbocharger. Experimental tests were also carried on a non-water cooled small diesel
177 engine turbocharger to see the difference in thermal transfers between the two. On the
178 turbocharger test bench, a first set of measurements is applied on the tested turbochargers
179 to generate a performance map close to the supplier map conditions. It is called
180 “reference” or “Ref” performance map. In these conditions, the turbine inlet temperature
181 is fixed at 500°C or 580°C (maximum temperature possible on the test bench) and the oil
182 inlet temperature is fixed at 90°C; the oil pressure is 3 bars. In the case of the water-

cooled turbocharger, the water inlet temperature is 80°C. On the compressor side, the air is sucked at ambient conditions.

The second set of measurements carried on the turbochargers are the "adiabatic" measurements. The "adiabatic" measurements are done to generate turbocharger performance maps with almost zero heat transfer. The turbocharger is insulated to minimize the heat transfers with the surrounding environment, and the average temperature in each component is kept to the minimum. The difference between the average temperatures of the different elements is also kept to a minimum. The lower limit for the temperature is at the turbine outlet to avoid frost. The average temperature equality is presented in equation (1). To control the average temperature in the turbine, compressor and central housing, the inlet temperatures are regulated for air going into the turbine and the compressor and the oil going into the central housing. In the case of the water-cooled turbocharger, the adiabatic measurements are done without water circulating. The temperatures are not very high in the turbine and cooling is not necessary: an important element in the thermal study is excluded to reduce the margin of error. Different adiabatic temperature hypothesis are studied: the average temperature equality in equation (1) is chosen; the different hypothesis are presented in details in the PhD thesis of G. Salameh [25].

$$\frac{T_{in,comp}+T_{out,comp}}{2}=\frac{T_{in,oil}+T_{out,oil}}{2}=\frac{T_{in,turb}+T_{out,turb}}{2} \quad (1)$$

A third set of measurements is carried on the water cooled turbocharger with different combinations of water and oil inlet temperatures. With the different temperatures combination (on the water and oil sides), reference conditions from the first set of measurements are applied on the air side in the turbine and compressor. The oil and

205 water temperatures are determined for each measurement. The results are shown in Fig. 5
206 to Fig. 12.

207 3 Model calculation

208 3.1 Model description

209 The thermal transfer model is based on the three lumped masses model by
210 Sanguinetti et al. [21]. The turbocharger is divided into three elements: turbine,
211 compressor and central housing. Each element exchanges heat with the fluid going
212 through it, the adjacent element or elements, and the surrounding environment (Fig. 2).
213 The difference in this model is the representation of the water cooling as a thermal
214 barrier. The compressor and the turbine heat transfer models can be separated and the
215 calculation becomes easier. The turbine heat transfer model can be applied without using
216 the compressor map and vice versa. The heat transfer models can be resumed by Fig. 2
217 and the equations (2) and (3). The lumped mass representing the central housing is
218 supposed at a uniform constant temperature T_{CH} for a steady state operating point. The
219 calculation of the central housing temperature is detailed in section 3.4.

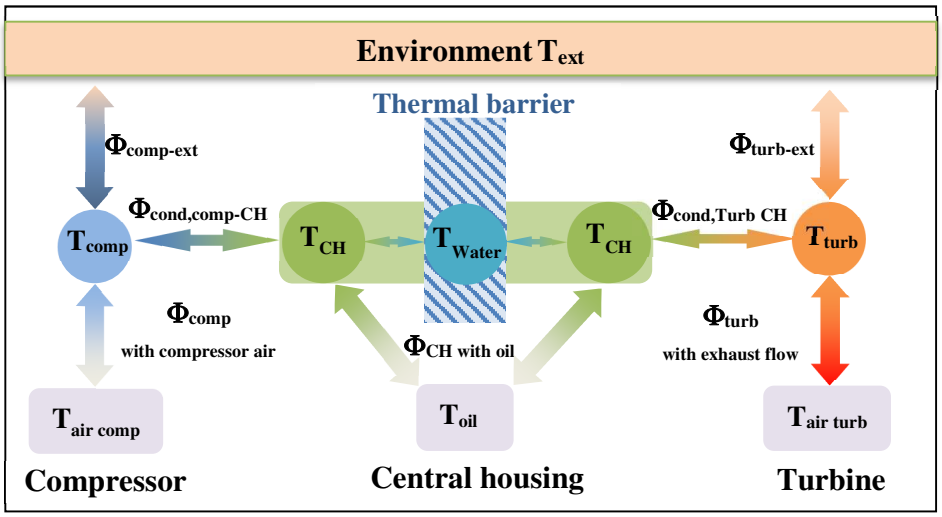

220

221 **Fig. 2.** Water-cooled turbocharger lump mass model

$$(mC)_{turb}\frac{\partial T_{turb}}{\partial t}=\Phi_{cond,turb-CH}+\Phi_{turb-\mathrm{int}}+\Phi_{turb-ext} \quad (2)$$

$$(mC)_{comp}\frac{\partial T_{comp}}{\partial t}=\Phi_{cond,comp-CH}+\Phi_{comp-\mathrm{int}}+\Phi_{comp-ext} \quad (3)$$

222 The heat transfer model is based on the model by Goumy et al. [22] for non-water-
223 cooled turbochargers. The turbine, compressor and central housing temperatures (T_{comp},
224 T_{turb} and T_{CH}) are the temperatures of the body of each element. In this model, every
225 element is considered as a one point mass with one uniform temperature. The external
226 heat transfers designated by $\Phi_{comp,ext}$ and $\Phi_{turb,ext}$ are the heat transfers between the
227 compressor and turbine bodies and the surrounding environment. The turbine external
228 transfer calculated in equation (4) could be divided into two types: convection and
229 radiation. In normal turbocharger operating conditions, only the turbine reaches
230 temperatures high enough to consider radiation. For the compressor external exchange,
231 only convection will be taken into consideration in equation (5) and the radiation effect is
232 neglected. The turbine is the more consequent element in terms of external losses as
233 mentioned by Payri et al. [26] and the radiation can be neglected for the other parts. The

234 external convection coefficients are not dependent on the operating point and hereby can
235 be fixed for all the calculation points.

$$\Phi_{turb-ext} = h_{ext,turb} S_{ext,turb} \left(T_{ext} - T_{turb}\right) - \varepsilon_{turb} S_{ext,turb} \sigma T_{turb}^4 \quad (4)$$

$$\Phi_{comp-ext} = h_{ext,comp} S_{ext,comp} \left(T_{ext} - T_{comp}\right) \quad (5)$$

236 The surrounding temperature T_{ext} is a constant measured in the test bench. The
237 external convection coefficients h_{ext} are constants designated according to the material
238 and the surrounding fluid. The external surface S_{ext} is a geometrical parameter calculated
239 based on the dimensions of the turbocharger as in the works of Goumy et al. [22]:
240 empirical equations are applied where the external surfaces and the distances are
241 calculated using a characteristic dimension: the impeller outer diameter. It works for the
242 compressor and the turbine.

243 The heat exchange between the adjacent elements is the conduction calculated in
244 equations (6) and (7) for the turbine and the compressor respectively. It is defined
245 according to the Fourrier's law as a function of the exchange surface and distance, the
246 material conductivity and the temperature difference. The metal conductivity λ_{iron} is a
247 constant characteristic of the material. The conduction surface areas $S_{turb\text{-}CH}$ and $S_{comp\text{-}CH}$
248 and the distances $e_{turb\text{-}CH}$ and $e_{comp\text{-}CH}$ are geometrical values determined as a function of
249 the turbocharger dimensions as mentioned above.

$$\Phi_{cond,turb-CH} = \frac{\lambda_{iron} S_{turb-CH}}{e_{turb-CH}} \left(T_{CH} - T_{turb}\right) \quad (6)$$

$$\Phi_{cond,comp-CH} = \frac{\lambda_{iron} S_{comp-CH}}{e_{comp-CH}} \left(T_{CH} - T_{comp}\right) \quad (7)$$

250 The exchange between the fluid going into the turbine and the compressor and the
251 body of each element is calculated in equations (8) and (9) using only convection. The

252 convection coefficient depends on the mass flow rate and has to be calculated for every
253 turbocharger operating point. In the turbine, the convection is considered before the
254 impeller. In the compressor it is considered after the impeller.

$$\Phi_{turb-\text{int}} = h_{\text{int},turb} S_{\text{int},turb} \left(T_{in,turb} - T_{turb} \right) \tag{8}$$

$$\Phi_{comp-\text{int}} = h_{\text{int},comp} S_{\text{int},comp} \left(T_{out,adia,comp} - T_{comp} \right) \tag{9}$$

255 The internal convection coefficient h_{int} is calculated in equation (10) as a function of
256 the fluid thermal conductivity λ calculated for air as a function of the pressure and the
257 temperature, the characteristic dimension of the flow L_c considered as the impeller outer
258 diameter for the turbine and the compressor, and the Nusselt number Nu calculated in
259 equation (11) using Gnielinski correlation [27] valid for smooth tubes over a large
260 Reynolds number range [28].

$$h_{\text{int}} = \frac{\lambda \times Nu}{L_c} \tag{10}$$

$$Nu = \frac{(f/8)(\text{Re}-1000)\text{Pr}}{1+12.7(f/8)^{0.5}\left(\text{Pr}^{2/3}-1\right)} \tag{11}$$

261 The variable f in the Nusselt equation is a function of the Reynolds number
262 calculated using equation (12). The Prandtl and Reynolds numbers are also calculated in
263 equations (13) and (14). For air, the cinematic and dynamic viscosities ν and μ are
264 calculated using the temperature and pressure.

$$f = \left(0.79\ln(\text{Re}) - 1.64\right)^{-2} \tag{12}$$

$$\text{Pr} = \frac{\mu(T) \times c_p}{\lambda} \tag{13}$$

$$\text{Re} = \frac{velocity \times L_c}{\nu} \tag{14}$$

3.2 Thermal barrier concept

In the case of the water cooled turbocharger, studies show that water cooling can be considered as a thermal barrier as mentioned by Cormerais et al. [17]: the heat transfers between the turbine and the compressor could be reduced and the only heat transfers remaining between the different components are between the turbine and the central housing and between the compressor and the central housing. The effect of the significant water flow rate and specific heat is that the central housing remains at a constant temperature and reduces the heat exchange between the turbine and the compressor. To see the effect of the water-cooling, two sets of experiments are carried. The operating conditions are the same for both sets except one difference: the turbine inlet temperature is 500°C in the first set and 100°C in the second set. For the compressor, oil and water inlet conditions, they are the same for the two sets. The results for the water-cooled turbocharger are showed in Fig. 3. The compressor efficiency is calculated using the inlet and outlet temperatures as shown in equation (19). Fig. 3 shows that, away from the boundary limits, the compressor isentropic efficiency does not mostly change with the turbine inlet temperature variation for the water cooled turbocharger.

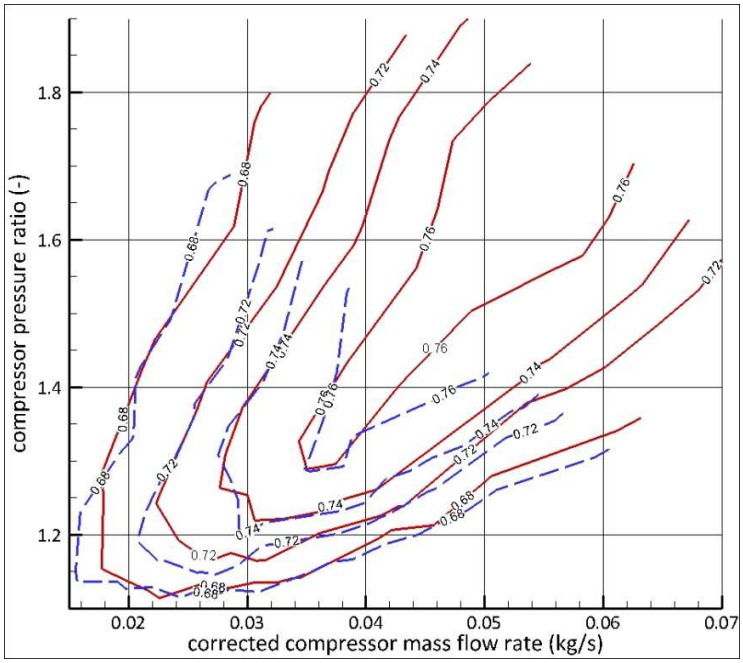

Fig. 3. Water cooled turbocharger compressor efficiency performance map: isentropic efficiency vs. corrected mass flow rate; turbine inlet temperature 500°C in red and turbine inlet temperature 100°C in dashed blue lines.

A non-water-cooled turbocharger is tested to see the effect of the turbine inlet temperature on the compressor efficiency without water cooling. Two series of measurements are carried: a first set of measurements with a turbine inlet temperature at 580°C and a second set of measurements at adiabatic conditions. The adiabatic conditions are presented in section 2: they are used in this part as "cold" measurement conditions to compare with "hot" measurements. The compressor efficiency is plotted in Fig. 4 for the two conditions. It shows that the compressor efficiency is highly affected by the turbine inlet temperature in this case. The heat transfers between the turbine and the compressor have an important impact on their performance. Compared to the results of the water-cooled turbocharger in Fig. 3, it can be considered that the water cooling reduces the effect of the turbine inlet temperature on the compressor performance: hereby the heat

transfers between the turbine and the compressor could then be neglected. The central housing is considered as one lumped mass at a constant uniform temperature which is a function the oil and water temperatures. This central housing temperature is not the real central housing measured temperature: it is an intermediate value used to calculate the turbine and compressor heat transfers.

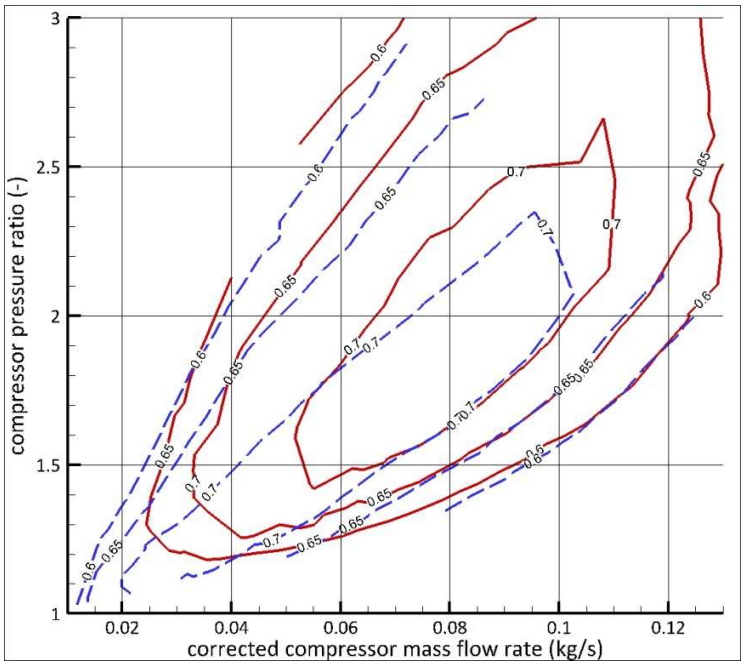

Fig. 4. Non water cooled turbocharger compressor efficiency performance map: isentropic efficiency vs. corrected mass flow rate; turbine inlet temperature 580°C in red and adiabatic measurements in dashed blue lines.

3.3 Turbocharger friction model

A part of the heat exchanged in the turbocharger is the heat produced from the friction of the moving parts. In this study, the friction power is converted entirely into heat going to the lubricating oil. The friction power is calculated using the model of Perrot et al. [29]. In their model, Perrot et al. [29] calculate the friction power as a function of the oil viscosity and the turbocharger regime as shown in equation (15) where “a” and “b” are

311 calibration coefficients; “a” is a constant determined by the experiments and “b” is
312 calculated as a function of the compressor impeller outer diameter.

$$P_{friction} = N^2 \times (a \times \mu + b) \times 10^{-8} \quad (15)$$

313 The oil viscosity μ is calculated using the oil inlet temperature $T_{oil,in}$ with the model of M.
314 Deligant [30] in equation (16). The coefficients “c”, “d” and “e” are determined
315 according to the type of oil used.

$$\mu(T) = c \times e^{\frac{d}{T+273.16-e}} \quad (16)$$

316 **3.4 Central housing temperature calculation**

317 Using the oil inlet temperature and the turbocharger rotational speed, and knowing the
318 type of oil used, the friction dissipated power can be calculated using equation (15). This
319 friction power being converted into heat going to the oil, and considering that the oil does
320 not exchange heat other than the one coming from the friction power, the oil outlet
321 temperature can be calculated in equation (17) knowing the oil mass flow rate and
322 specific heat.

$$T_{out,oil} = T_{in,oil} + \frac{P_{friction}}{\dot{m}_{oil} \times c_{oil}} \quad (17)$$

323 For the lump mass model, the central housing temperature is calculated using the oil
324 outlet temperature and the cooling water inlet temperature as shown in equation (18).
325 Since the water flow rate and specific heat are significant, the central housing is
326 considered at a stabilized thermal point with a constant temperature. The central housing
327 temperature is a representative value of the heat transfers occurring in the central
328 housing. It is not a real temperature because the central housing does not have a uniform
329 temperature in all its regions. The coefficient “k” shown in equation (18) is a constant

330 equal to 0.25 and determined using experimental measurements at different oil and water
331 temperatures combinations.

$$T_{CH} = k \times T_{water} + (1-k) T_{out,oil} \tag{18}$$

332 The data shown in Fig. 5 to Fig. 12 represents the compressor isentropic
333 efficiency calculated at different water and oil temperatures combinations with the same
334 model calibration for the central housing temperature calculation. The reference
335 conditions ("ref") points are the data measured with hot air going through the turbine and
336 atmospheric air going through the compressor as described in section 2. The oil and water
337 temperatures are different for every set of points. The adiabatic measurements ("adia")
338 are the measurements with controlled turbine and compressor inlet temperatures. The
339 detailed description of the adiabatic measurements is presented in section 2 based on the
340 works of Salameh et al. [24][25]. These measurements are done to calculate the
341 compressor efficiency using the reference measurement conditions and the heat transfer
342 model with the central housing temperature calculation. The "model" results are
343 compared to the adiabatic measurements to validate the calculation of the central housing
344 temperature using equation (18).

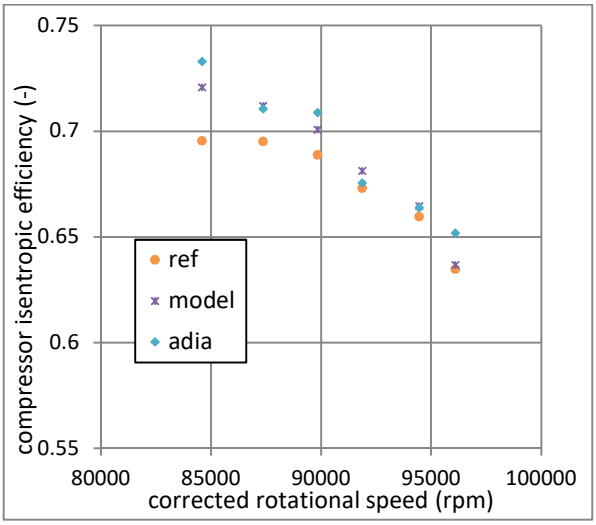

345

346 **Fig. 5.** Compressor efficiency vs. corrected rotational speed for water inlet temperature
347 50°C and oil inlet temperature 50°C: reference conditions points, adiabatic experimental
348 points and heat transfer model points. Turbocharger regime range from 80 000 rpm to
349 100 000 rpm.

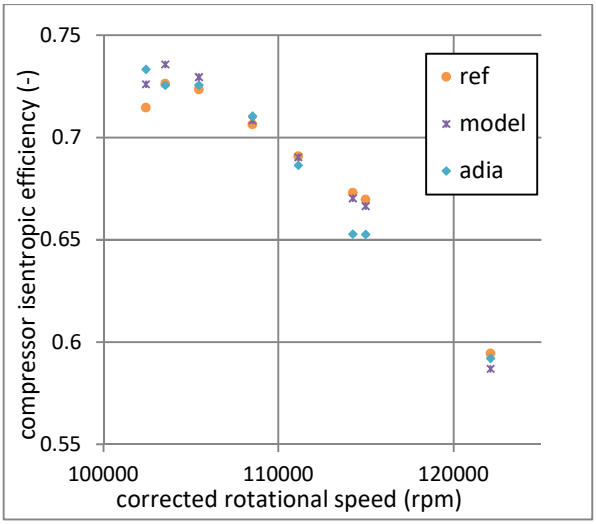

350

351 **Fig. 6.** Compressor efficiency vs. corrected rotational speed for water inlet temperature
352 50°C and oil inlet temperature 50°C: reference conditions points, adiabatic experimental
353 points and heat transfer model points. Turbocharger regime range from 100 000 rpm to
354 125 000 rpm.

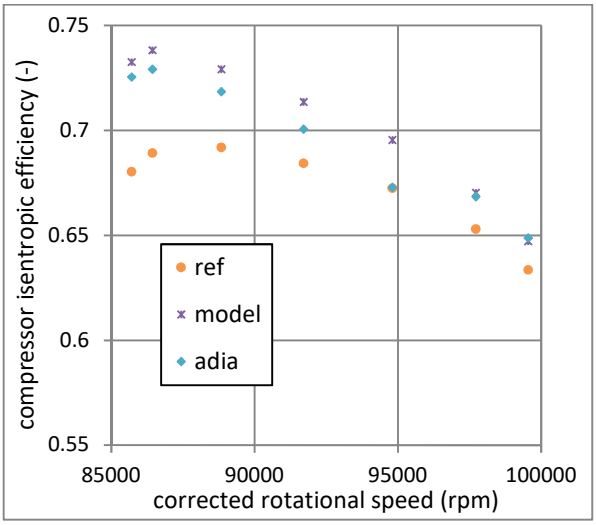

355

356 **Fig. 7.** Compressor efficiency vs. corrected rotational speed for water inlet temperature
357 50°C and oil inlet temperature 70°C: reference conditions points, adiabatic experimental
358 points and heat transfer model points. Turbocharger regime range from 85 000 rpm to
359 100 000 rpm.

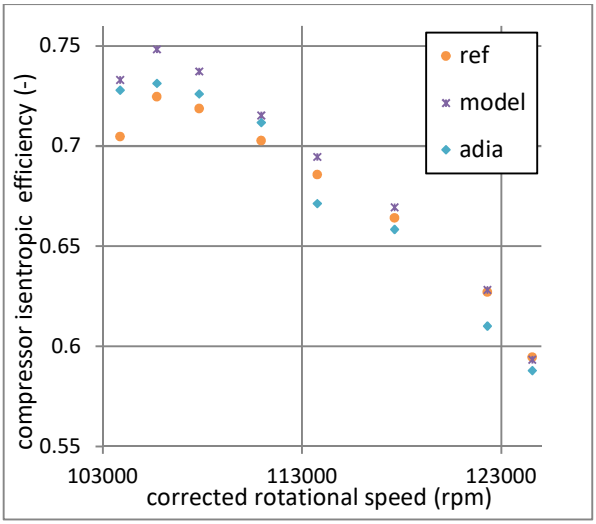

360

361 **Fig. 8.** Compressor efficiency vs. corrected rotational speed for water inlet temperature
362 50°C and oil inlet temperature 70°C: reference conditions points, adiabatic experimental
363 points and heat transfer model points. Turbocharger regime range from 100 000 rpm to
364 125 000 rpm.

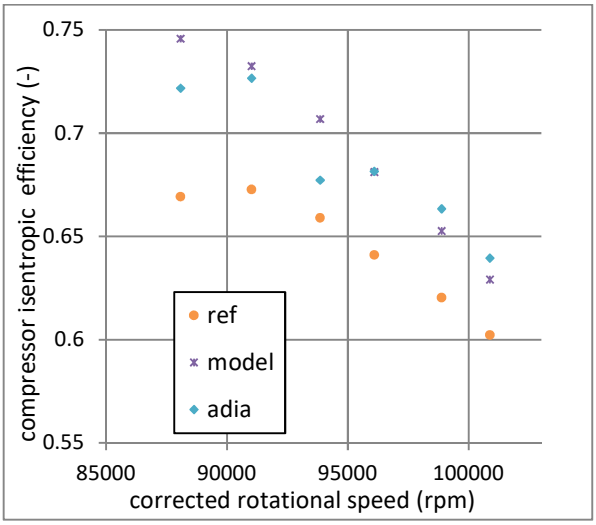

365

366 **Fig. 9.** Compressor efficiency vs. corrected rotational speed for water inlet temperature
367 75°C and oil inlet temperature 90°C: reference conditions points, adiabatic experimental
368 points and heat transfer model points. Turbocharger regime range from 85 000 rpm to
369 100 000 rpm.

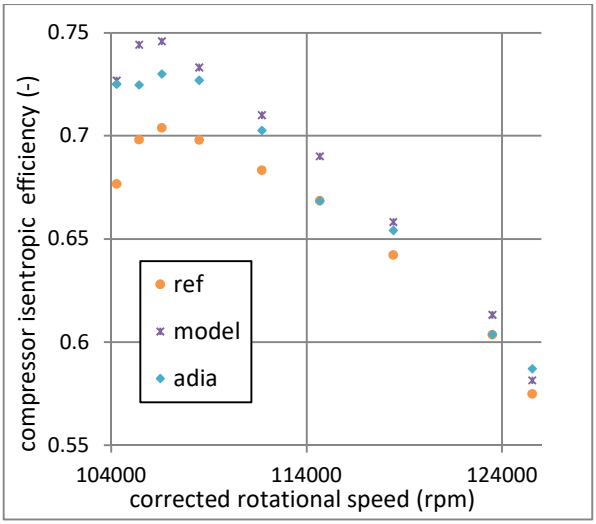

370

371 **Fig. 10.** Compressor efficiency vs. corrected rotational speed for water inlet temperature
372 75°C and oil inlet temperature 90°C: reference conditions points, adiabatic experimental
373 points and heat transfer model points. Turbocharger regime range from 100 000 rpm to
374 125 000 rpm.

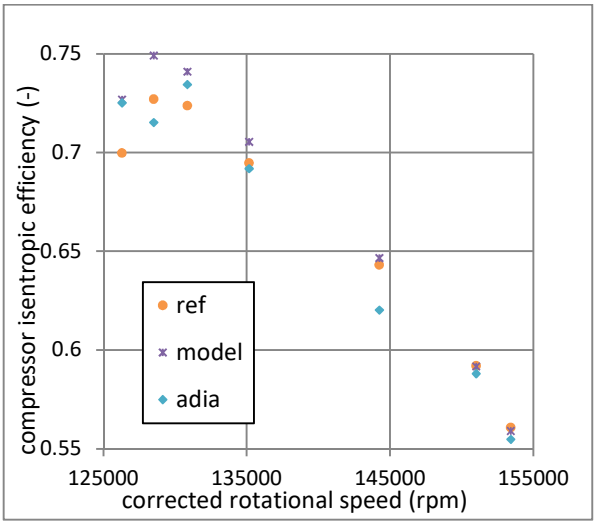

375

376 **Fig. 11.** Compressor efficiency vs. corrected rotational speed for water inlet temperature
377 75°C and oil inlet temperature 90°C: reference conditions points, adiabatic experimental
378 points and heat transfer model points. Turbocharger regime range from 125 000 rpm to
379 150 000 rpm.

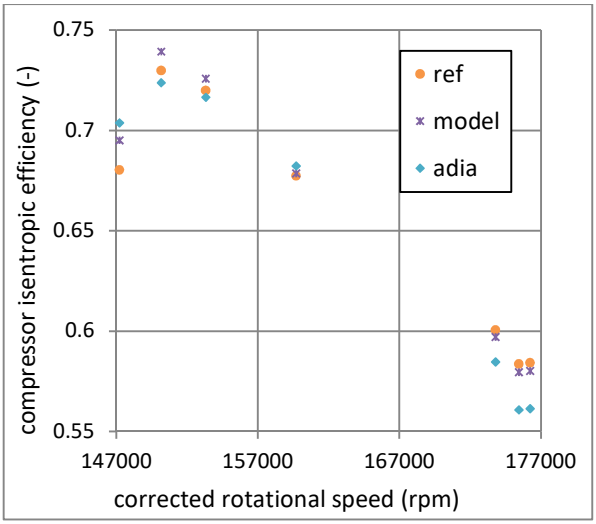

380

381 **Fig. 12.** Compressor efficiency vs. corrected rotational speed for water inlet temperature
382 75°C and oil inlet temperature 90°C: reference conditions points, adiabatic experimental
383 points and heat transfer model points. Turbocharger regime range from 150 000 rpm to
384 180 000 rpm.

385 Oil and water temperature combinations (50-50, 70-50, and 90-75) are used to check the
386 validity of the heat transfer model and specifically the central housing temperature
387 calculation using the value of the coefficient *k* in equation (18). When applying the heat
388 transfer model to the reference conditions measurements, the compressor efficiency gets
389 closer to the adiabatic measurements data. The heat transfer model is then working in the
390 right direction. At higher rotational speeds, the gap between the "ref" data and the "adia"
391 data is narrowed due to the decrease in the relative ratio of the heat transfer to the
392 mechanical power exchanged. The model has a better performance on the data at 75°C
393 for water and 90°C for oil: this set of data is the most important to take into consideration
394 because these conditions are the closest to the reference or real operating conditions.

395 **4 Turbocharger adiabatic maps generation:**

396 The performance map of a turbocharger given by the supplier is calculated in hot
397 conditions: the turbine inlet temperature is above 600°C, the oil inlet temperature is
398 around 90°C and the water inlet temperature is around 80°C when the turbocharger is
399 water-cooled. The equations used to calculate the compressor and the turbine efficiencies
400 are based on the first law of thermodynamics applied on a steady-state flow of an ideal
401 gas through an adiabatic process in an open system. With the temperature gradients
402 mentioned above, and the turbocharger not being insulated, the process in both the
403 turbine and the compressor is far from adiabatic. It is then necessary to quantify the heat
404 transfers in every element and calculate the correct power and hereby the correct
405 efficiency. The compressor isentropic efficiency is calculated in equation (19) using the
406 compressor inlet and outlet temperatures and the isentropic expansion outlet temperature

(calculated using the Laplace equation). The turbine supplier efficiency calculated in equation (22) is not the turbine isentropic efficiency: it is the ratio of the compressor adiabatic power to the turbine isentropic available power. It is then the product of the turbine isentropic efficiency (equation (20)) by the turbocharger mechanical efficiency (equation (21)).

$$\eta_{adia,\exp,comp} = \frac{w_{comp,isentr}}{w_{comp}} = \frac{T_{in,comp}\left(\tau_{comp}^{\frac{\gamma-1}{\gamma}} - 1\right)}{T_{out,comp} - T_{in,comp}} \quad (19)$$

$$\eta_{adia,\exp,turb} = \frac{w_{turb}}{w_{turb,isentr}} = \frac{T_{in,turb} - T_{out,turb}}{T_{in,turb}\left(1 - \tau_{turb}^{\frac{\gamma-1}{\gamma}}\right)} \quad (20)$$

$$\eta_{mech} = \frac{\dot{m}_{comp} \times c_p \times \left(T_{out,comp} - T_{in,comp}\right)}{\dot{m}_{turb} \times c_p \times \left(T_{in,turb} - T_{out,turb}\right)} \quad (21)$$

$$\eta_{turb} = \frac{\dot{m}_{comp} \times c_p \times \left(T_{out,comp} - T_{in,comp}\right)}{\dot{m}_{turb} \times c_p \times T_{in,turb}\left(1 - \tau_{turb}^{\frac{\gamma-1}{\gamma}}\right)} \quad (22)$$

These equations ((19) to (22)) are correct if the process is adiabatic in both the turbine and the compressor. It is then necessary to reevaluate these efficiencies taking into account the mechanical powers and the heat exchanges. With the water cooling, the heat transfers can be evaluated in the turbine and the compressor separately and the adiabatic performance maps can be generated using the supplier performance map of the studied element (turbine or compressor) without the other.

4.1 Compressor adiabatic map generation:

A supplier compressor performance map is measured on a conventional turbocharger test bench with high temperatures at the turbine inlet and also relatively hot

421 water and oil. The data is recorded for thermally stabilized operating points. The
422 compressor heat transfer balance presented in the differential equation (3) becomes:

$$\Phi_{cond,comp-CH} + \Phi_{comp-\mathrm{int}} + \Phi_{comp-ext} = 0 \tag{23}$$

423 The enthalpy power calculated using the compressor inlet and outlet temperatures
424 can be calculated using the supplier map data: the compressor inlet temperature, the
425 pressure ratio, the efficiency, the mass flow rate and the specific heat:

$$P_{enth,comp} = \dot{m}_{comp}\Delta h_{comp} = \frac{\dot{m}_{comp} \times c_{p,comp} \times T_{in,comp}}{\eta_{\mathrm{sup},comp}} \left(\tau_{comp}^{\frac{\gamma-1}{\gamma}} - 1 \right) \tag{24}$$

426 In this case, the enthalpy power is separated from the mechanical power because
427 of the heat transfers that must be taken into consideration:

$$P_{enth,comp} = P_{mecha,comp} - \Phi_{comp-\mathrm{int}} \tag{25}$$

428 The mechanical power is the power produced or consumed due to the moving parts
429 (impeller). In this study, the heat transfers do not take place in the impellers so the
430 mechanical power can be calculated using the impellers inlet and outlet temperatures.
431 If the heat transfer with the fluid inside the compressor can be modeled after the
432 impeller, another temperature can be calculated: the compressor impeller adiabatic outlet
433 temperature $T_{out,adia,comp}$: this temperature is the temperature at the impeller outlet if the
434 heat transfer is applied only after the impeller. The impeller adiabatic outlet temperature
435 can be used to calculate the compressor mechanical consumed power:

$$P_{mecha,comp} = \dot{m}_{comp} \times c_{p,comp} \times \left(T_{out,adia,comp} - T_{in,comp} \right) \tag{26}$$

436 The system of equations (5), (7), (9), (23), (24), (25) and (26) can be solved and
437 the results are the compressor body temperature T_{comp}, the impeller adiabatic outlet
438 temperature $T_{out,adia,comp}$ and the compressor internal heat exchange $\Phi_{comp\text{-}int}$. The
439 compressor adiabatic efficiency calculated in equation (19) in adiabatic conditions can be

calculated in this case but when taking into account the heat transfers. The combination of the efficiency definition and the equations (23) to (26) gives the following equation allowing the calculation of the compressor adiabatic efficiency in non-adiabatic measurement conditions:

$$\eta_{adia,comp,\mathrm{mod}el} = \left(\frac{1}{\eta_{\mathrm{sup},comp}} + \frac{\Phi_{comp-\mathrm{int}}}{\dot{m}_{comp} \times c_{p,comp} \times T_{in,comp} \left(\tau_{comp}^{\frac{\gamma-1}{\gamma}} - 1 \right)} \right)^{-1} \quad (27)$$

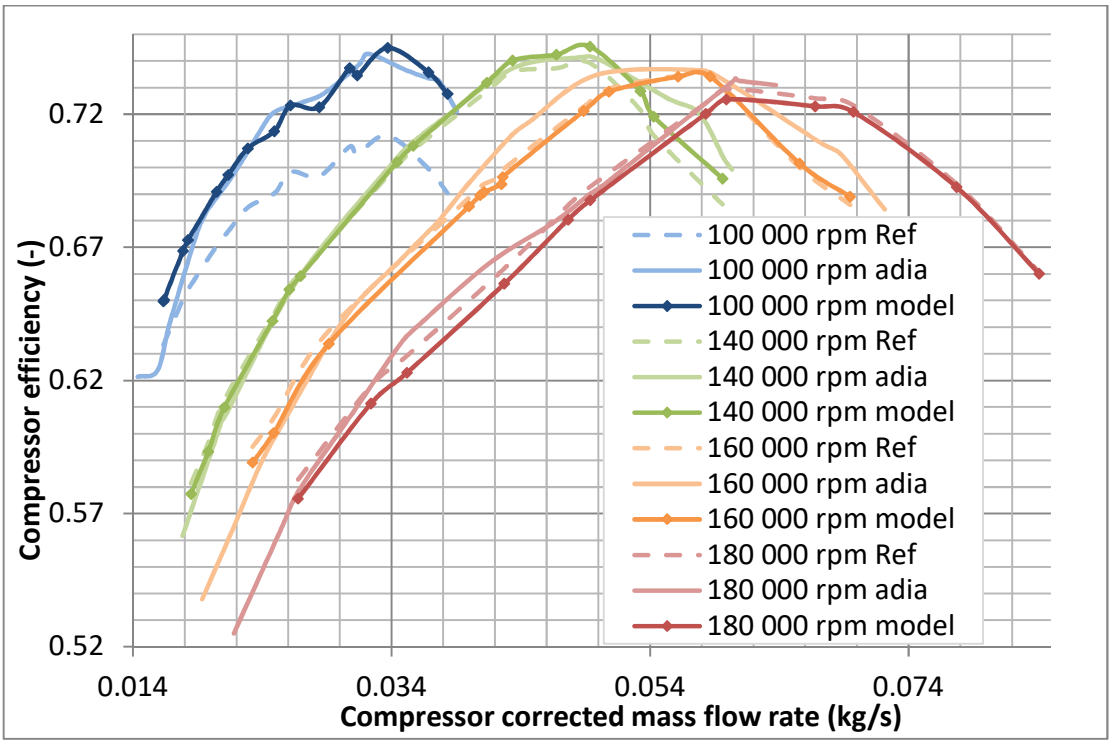

Fig. 13. Compressor efficiency curves for different corrected rotational speeds: Reference map conditions, experimental adiabatic conditions and heat transfer model results.

The results shown in Fig. 13 are three series: the reference map conditions data measured on the hot test bench, the adiabatic conditions experimental data and the points calculated using the reference map and the heat transfer model; the last set is named "model" because of the heat transfer model applied. The results are plotted in constant

451 regime curves for the three different conditions. The curves are set from left to right in
452 the growing rotational speed direction. The reference map data are the dashed lines, the
453 adiabatic data are the light colored lines, and the heat transfer model results are the lines
454 with dots. It can be seen that the heat transfer has a greater effect on the compressor
455 efficiency at lower rotational speeds. The difference is obvious between the reference
456 data and the adiabatic data at lower rotational speeds. At higher rotational speeds, the
457 effect of the heat transfer on the compressor efficiency is reduced. The amount of heat
458 exchanged can increase but its relative ratio to the mechanical power exchanged between
459 the turbine and the compressor is greatly reduced. At high rotational speeds, the curves of
460 the reference and adiabatic data become almost one. The heat transfer is calculated but its
461 amount does not change the compressor efficiency value.

462 **4.2 Turbine adiabatic map generation:**

463 A supplier turbine performance map is measured on a conventional turbocharger
464 test bench with high temperatures at the turbine inlet and also relatively hot water and oil.
465 The data is recorded for thermally stabilized operating points. The heat transfers are
466 between the body and the following elements: the surrounding environment (radiation
467 and convection), the central housing (conduction) and the internal turbine fluid
468 (convection) as shown in Fig. 2. The differential equation (2) becomes:

$$\Phi_{cond,turb-CH} + \Phi_{turb-\mathrm{int}} + \Phi_{turb-ext} = 0 \tag{28}$$

469 On the turbine side, the approach is close from the one applied for the compressor.
470 Due to water-cooling, the turbine heat transfer model can be applied without taking into
471 account the heat transfers between the turbine and the compressor. However, the

compressor map must be used to calculate the mechanical power delivered by the turbine at every operating point since the turbine supplier efficiency is the ratio of the compressor enthalpy power to the turbine isentropic enthalpy power as detailed in equation (22).

Knowing the values of the turbine inlet air temperature $T_{in,turb}$, the surrounding air temperature T_{ext}, and the central housing temperature T_{CH} calculated in section 3.4, it is possible to calculate the turbine body temperature $T_{in,turb}$ using the equations (4), (6), (8) and (28). With the value of the turbine body temperature $T_{in,turb}$, the turbine heat fluxes can be calculated and the impeller inlet temperature $T_{in,imp,turb}$ can be calculated considering that the heat transfers occur only before the impeller:

$$\Phi_{turb-\mathrm{int}} = \dot{m}_{turb} \times c_p \left(T_{in,turb} - T_{in,imp,turb} \right) \tag{29}$$

The compressor enthalpy power $P_{enth,comp}$ can be calculated using only the turbine supplier map: the turbine efficiency can be used to calculate the compressor enthalpy power in equation (22). As for the compressor, the mechanical power is the power produced or consumed due to the moving parts (impeller). In this study, the heat transfers do not take place in the impellers so the mechanical powers can be calculated using the impellers inlet and outlet temperatures. The compressor mechanical power $P_{mecha,comp}$ can be calculated using equation (25). For this, it is necessary to know the compressor enthalpy power $P_{enth,comp}$ and the compressor internal heat exchange $\Phi_{comp\text{-}int}$. To know the compressor internal heat transfer, compressor data from the previous section must be plotted in a map: with the turbine characteristics, every operating point is designated and placed in the compressor map to evaluate the compressor internal heat transfer. Another approach can be applied at this step: the compressor internal heat flux can be neglected $\Phi_{comp\text{-}int}$ in the turbine adiabatic map generation: its influence is not significant on the

494 results. It becomes possible to avoid using the compressor data map for the turbine
495 calculation. The results for the two approaches (with and without compressor internal
496 heat transfer $\Phi_{comp\text{-}int}$) are shown in Fig. 14 and Fig. 15 and it confirms the possibility of
497 not taking into account the compressor internal heat transfer in the turbine heat transfer
498 calculations.

499 There are three series of turbine outlet temperatures: $T_{out,turb,expe}$, $T_{out,turb,model}$, and
500 $T_{out,turb,without\ heat\ transfer}$. $T_{out,turb,expe}$ is the experimental temperature measured at the turbine
501 outlet when operating in "hot" conditions. $T_{out,turb,model}$ is the turbine outlet temperature
502 calculated using the inlet conditions and the heat transfer model developed in this study:
503 it should match the data from the $T_{out,turb,expe}$ series. $T_{out,turb,without\ heat\ transfer}$ is the turbine
504 outlet temperature calculated using the inlet conditions and without a heat transfer model
505 applied. The difference between $T_{out,turb,expe}$ and $T_{out,turb,without\ heat\ transfer}$ shows the
506 importance of a heat transfer model in these conditions.

507 The friction power $P_{friction}$ calculated in equation (15) can be added to the
508 compressor mechanical power $P_{mecha,comp}$ to calculate the turbine mechanical power
509 $P_{mecha,turb}$ (equation (30)). The turbine outlet temperature is then calculated using the
510 turbine mechanical power and the turbine impeller inlet temperature as shown in equation
511 (31).

$$P_{mecha,turb} = P_{mecha,comp} + P_{friction} \tag{30}$$

$$P_{mecha,turb} = \dot{m}_{turb} \times c_p \left(T_{in,imp,turb} - T_{out,turb} \right) \tag{31}$$

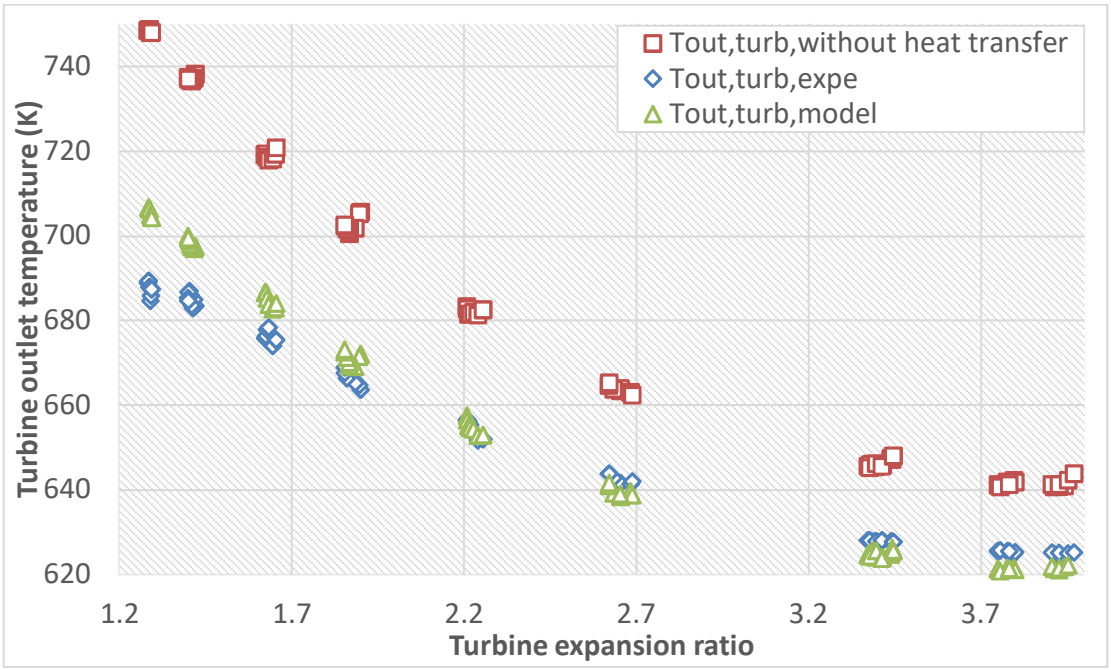

512

513 **Fig. 14.** Turbine outlet temperatures with compressor internal heat transfer: Turbine
514 outlet temperature calculated with heat transfer, without heat transfer and experimentally
515 measured turbine outlet temperature

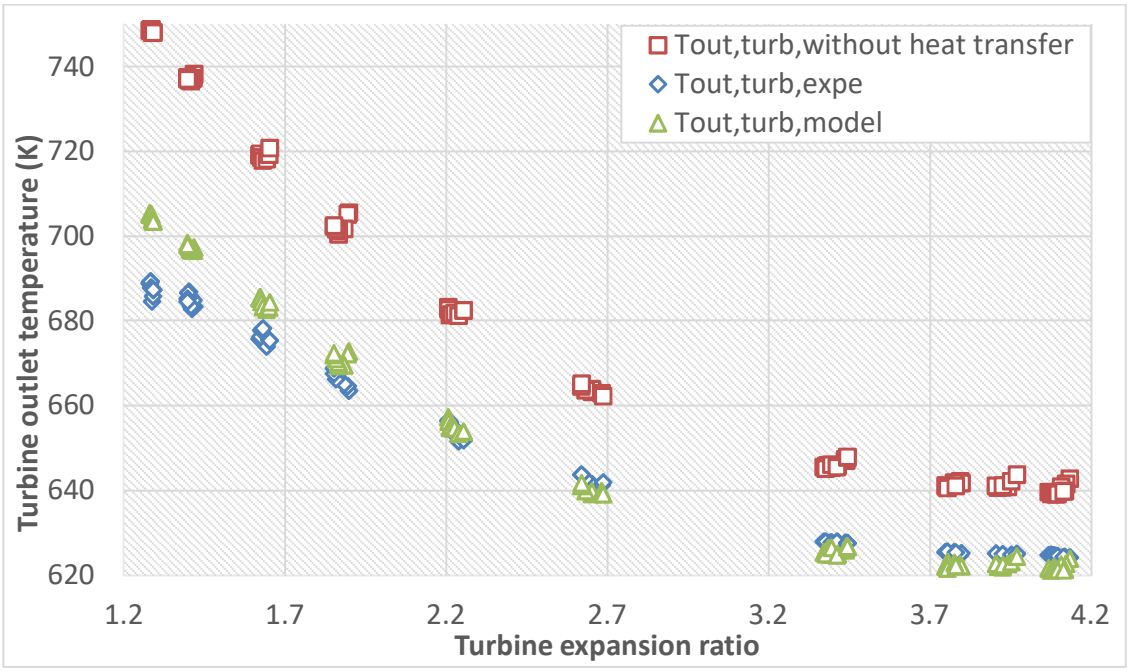

Fig. 15. Turbine outlet temperatures without compressor internal heat transfer: Turbine outlet temperature calculated with heat transfer, without heat transfer and experimentally measured turbine outlet temperature.

As shown in Fig. 14 and Fig. 15, it is possible to neglect the effect of the compressor internal heat flux in the turbine heat transfer calculation. The results from Fig. 15 will be considered as final results.

The effect of applying the heat transfer model is obvious and the results show a temperature difference up to 63 K between the experimental data and the data calculated without the heat transfers: this represents a 9.2% difference. The maximum difference between the experimental data in adiabatic conditions and the one calculated with the heat transfer model is 20 K or 2.9%. The Mean Absolute Error (MAE) defined in equation (32) is 6 and the coefficient of determination (R^2) defined in equation (33) is 0.89.

$$MAE = \frac{1}{Nbre}\sum_{i=1}^{Nbre}\left|\frac{T_{out,turb,model} - T_{out,turb,expe}}{T_{out,turb,expe}}\right| \quad (32)$$

$$R^2 = 1 - \frac{\sum_{i=1}^{Nbre}\left[T_{out,turb,model} - T_{out,turb,expe}\right]^2}{\sum_{i=1}^{Nbre}\left[T_{out,turb,expe} - T_{mean,out,turb,expe}\right]^2} \quad (33)$$

530 Once the turbine outlet temperature $T_{out,turb,model}$ is calculated, it is possible to
531 calculate the turbine isentropic efficiency as in equation (20). In this case, the values are
532 not adiabatic measurement temperatures but calculated using the heat transfer model; the
533 turbine isentropic efficiency equation becomes:

$$\eta_{isentr,turb} = \frac{T_{in,turb} - T_{out,turb,model}}{T_{in,turb}\left(1 - \tau_{turb}^{\frac{\gamma-1}{\gamma}}\right)} \quad (34)$$

534 The different efficiencies are plotted in Fig. 16. The turbine supplier efficiency is
535 the ratio of the compressor enthalpy difference to the turbine isentropic enthalpy
536 difference as in equation (22). The supplier enthalpy ratio is not an efficiency but the
537 ratio of the turbine enthalpy difference to the turbine isentropic enthalpy difference; it is
538 calculated with the same equation (34) but with a turbine outlet temperature calculated
539 without heat transfer. The calculation is shown in equation (35). The supplier enthalpy
540 ratio is calculated to show the effect of the heat transfers on the calculation of
541 efficiencies: the equation used to calculate the efficiency with the temperature difference
542 is true for an adiabatic flow so the heat transfers must be evaluated and removed from the
543 enthalpy difference. The turbine isentropic efficiency calculated using the turbine outlet
544 temperature from the heat transfer model (equation (34)) is also plotted. The turbocharger
545 mechanical efficiency is calculated using only the turbine performance map: the friction
546 power is evaluated using the model from section 3.3 and the turbine mechanical power is
547 calculated using equation (31). The turbocharger mechanical efficiency is the ratio of the

548 compressor mechanical power to the turbine mechanical power; the compressor
549 mechanical power being the difference between the turbine mechanical power and the
550 friction power. The mechanical efficiency is calculated using equation (36).

$$Supplier-enthalpy-ratio=\frac{T_{in,turb}-T_{out,turb,without-heat-transfer}}{T_{in,turb}\left(1-\tau_{turb}^{\frac{\gamma-1}{\gamma}}\right)} \quad (35)$$

$$\eta_{mecha}=\frac{P_{mecha,comp}}{P_{mecha,turb}}=\frac{P_{mecha,turb}-P_{friction}}{P_{mecha,turb}} \quad (36)$$

551

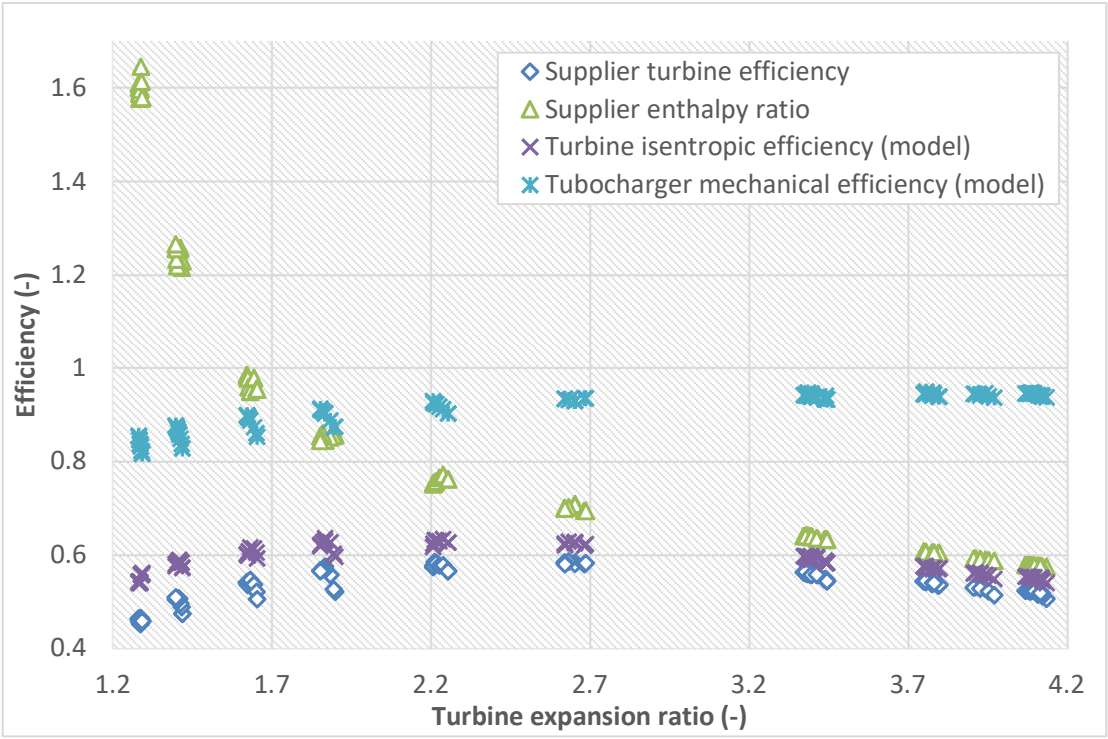

552

553 **Fig. 16.** Turbine efficiencies: supplier turbine efficiency, supplier enthalpy ratio, turbine
554 isentropic efficiency (model), turbine mechanical efficiency (model)

555 **5 Conclusions**

556 A heat transfer model for the compressor and the turbine of a water-cooled
557 turbocharger is presented. This study separates the heat transfer models of the turbine and

558 the compressor. The calculation on each side can be done separately from the other one.
559 Water-cooling can be considered as a thermal barrier allowing the heat transfers to be
560 separated on the turbine and the compressor sides. The compressor heat exchange is
561 between the compressor and the central housing, the internal flow and the surrounding
562 environment. The turbine heat exchange is also between the turbine and the central
563 housing, the internal flow and the surrounding environment. The radiation is only
564 considered on the turbine side due to high temperatures. The central housing is
565 considered at a uniform constant temperature at stabilized operation points. To separate
566 the calculation on the compressor side and the turbine side, the friction power is
567 calculated based on the oil temperature and the turbocharger regime. The friction power
568 is entirely transferred to the oil in the central housing as heat and the oil outlet
569 temperature is calculated. The central housing temperature is calculated using the oil and
570 water temperatures based on a set of measurements at different conditions.

571 The heat transfer model applied on a compressor or a turbine performance map
572 generates a new map at adiabatic conditions. The points from the map are measured at
573 stabilized points and different temperature gradients in the turbine, the compressor and
574 the central housing. The heat transfer model on the compressor side generates an
575 efficiency map in adiabatic conditions to correct the supplier efficiency calculated with
576 non-adiabatic data. The effect of the heat transfer on the compressor efficiency is more
577 significant at low rotational speeds and due to its relatively high ratio in the power
578 exchanged. At higher rotational speeds; the heat transfer has a lower effect on the
579 compressor efficiency even though the heat flux increases but the mechanical power
580 exchanged increases much more and makes the heat transfer insignificant.

On the turbine side, the heat transfer is applied to calculate the turbine impeller inlet temperature considering the heat exchange taking place before the impeller. The turbine mechanical power is calculated using the compressor mechanical power and the friction power. The compressor mechanical power is calculated using the supplier turbine efficiency and the expansion ratio and the compressor heat exchange is neglected in the calculation of the compressor power. The turbine mechanical power is then calculated and so is the turbine outlet temperature. This temperature is compared to the experimental values and to the turbine outlet temperature calculated without heat exchanges. Using the temperatures calculated the turbine efficiencies are plotted: the turbine isentropic (adiabatic) efficiency, the turbocharger mechanical efficiency and the turbine supplier efficiency.

The advantages of this model are its simplicity and the capability of doing the calculation on the compressor and the turbine separately without having to couple the operating points or use the performance map of the other element. In this study, adiabatic efficiency maps are plotted for thermally stabilized steady-state points and the next step could be to implement this model into a software and apply it on transient operating conditions.

ACKNOWLEDGMENT

The authors wish to acknowledge Renault, Siemens and Ecole Centrale de Nantes, members of the industrial chair “system modeling for the control and calibration of internal combustion engines” for their technical support to this project.

602 **FUNDING**

603 This research did not receive any specific grant from funding agencies in the public,

604 commercial, or not-for-profit sectors.

605 **NOMENCLATURE**

a, b, c, d, e, f, k	coefficients [-]
c_p	Air thermal capacity [J.kg^{-1}.K^{-1}]
c_{oil}	Oil thermal capacity [J.kg^{-1}.K^{-1}]
Δh_{comp}	Compressor enthalpy difference [J.kg^{-1}]
$e_{comp\text{-}CH}$	Thickness between compressor and central housing [m]
$e_{turb\text{-}CH}$	Thickness between turbine and central housing [m]
$h_{int,comp}$	Compressor internal convection coefficient [W.m^{-2}.K^{-1}]
$h_{ext,comp}$	Compressor external convection coefficient [W.m^{-2}.K^{-1}]
$h_{int,turb}$	Turbine internal convection coefficient [W.m^{-2}.K^{-1}]
$h_{ext,turb}$	Turbine external convection coefficient [W.m^{-2}.K^{-1}]
i	Number [-]
L_c	Characteristic dimension: impeller outer diameter [m]
MAE	Mean Absolute Error [-]
mC	Thermal inertia [J.K^{-1}]
$\dot{m}$	Mass flow rate [kg.s^{-1}]
$\dot{m}_{comp}$	Compressor mass flow rate [kg.s^{-1}]
$\dot{m}_{turb}$	Turbine mass flow rate [kg.s^{-1}]

$\dot{m}_{oil}$	Oil mass flow rate [kg.s^{-1}]
$Nbre$	Number of data points [-]
N	Turbocharger rotational speed [rpm]
Nu	Nusselt number [-]
P	Pressure [Pa]
$P_{friction}$	Friction power [W]
$P_{enth,comp}$	Compressor enthalpy power [W]
$P_{mecha,comp}$	Compressor mechanical power [W]
$P_{enth,turb}$	Turbine mechanical power [W]
Pr	Prandtl number [-]
R^2	Coefficient of determination [-]
Re	Reynolds number [-]
$S_{ext,comp}$	Compressor external surface [m^2]
$S_{int,comp}$	Compressor internal surface [m^2]
$S_{comp-CH}$	Surface exchange between compressor and central housing [m^2]
$S_{ext,turb}$	Turbine external surface [m^2]
$S_{int,turb}$	Turbine internal surface [m^2]
$S_{turb-CH}$	Surface exchange between turbine and central housing [m^2]

t	Time [s]
T	Temperature [K]
T_{comp}	Compressor temperature [K]
$T_{in,comp}$	Compressor inlet temperature [K]
$T_{out,comp}$	Compressor outlet temperature [K]
$T_{out,adia,comp}$	Compressor outlet temperature without thermal transfer [K]
$T_{air,comp}$	Compressor air temperature [K]
T_{turb}	Turbine temperature [K]
$T_{in,turb}$	Turbine inlet temperature [K]
$T_{in,imp,turb}$	Turbine impeller inlet temperature [K]
$T_{out,turb}$	Turbine outlet temperature [K]
$T_{out,turb,expe}$	Turbine experimental outlet temperature [K]
$T_{out,turb,model}$	Turbine model outlet temperature [K]
$T_{out,turb,without\ heat\ transfer}$	Turbine outlet temperature without the heat transfer calculation [K]
$T_{air,turb}$	Turbine air temperature [K]
T_{oil}	Oil temperature [K]
$T_{in,oil}$	Oil inlet temperature [K]
$T_{out,oil}$	Oil outlet temperature [K]

T_{water}	Water inlet temperature [K]
T_{CH}	Central housing temperature [K]
T_{ext}	Ambient temperature [K]
w	Specific work [J/kg]
Greek symbols	
γ	Specific heat ratio [-]
ε_{turb}	Turbine emissivity [-]
$\eta_{adia,exp,comp}$	Compressor experimental adiabatic efficiency [-]
$\eta_{adia,exp,turb}$	Compressor experimental adiabatic efficiency [-]
$\eta_{adia,comp,model}$	Compressor model adiabatic efficiency [-]
$\eta_{sup,comp}$	Compressor supplier efficiency [-]
$\eta_{isentr,turb}$	Turbine isentropic efficiency [-]
η_{mech}	Turbocharger mechanical efficiency [-]
η_{turb}	Turbine efficiency (turbine isentropic x mechanical) [-]
λ	Fluid thermal conductivity [$W.m^{-1}.K^{-1}$]
λ_{iron}	Iron thermal conductivity [$W.m^{-1}.K^{-1}$]
μ	Fluid dynamic viscosity [$kg.m^{-1}.s^{-1}$]
σ	Stefan constant [$W.m^{-2}.K^{-4}$]

τ_{comp}	Compressor compression ratio [-]
τ_{turb}	Turbine expansion ratio [-]
v	Fluid kinematic viscosity [$kg.m^{-1}.s^{-1}$]
$\Phi_{turb\text{-}ext}$	Turbine external heat transfer [W]
$\Phi_{comp\text{-}ext}$	Compressor external heat transfer [W]
$\Phi_{cond,comp\text{-}CH}$	Conduction heat transfer between compressor and central housing [W]
$\Phi_{cond,turb\text{-}CH}$	Conduction heat transfer between turbine and central housing [W]
Φ_{turb}	Turbine internal heat transfer [W]
Φ_{comp}	Compressor internal heat transfer [W]
$\Phi_{CH\ with\ oil}$	Convection heat transfer between oil and central housing [W]
Subscripts	
adia	adiabatic
comp	compressor
enth	enthalpic
exp	experimental
ext	external
imp	impeller

in	inlet
mech	mechanical
oil	oil
out	outlet
ref	reference
sup	supplier
turb	turbine
Abbreviation	
ECU	Engine control unit
HIL	hardware in the loop

606

REFERENCES

[1] Hoffmann S, Gellineck S, Martin J, Mead S. Electric Supercharging and Hybridization with 12 V. MTZ Worldw 2018;79:16–23. https://doi.org/10.1007/s38313-018-0017-5.

[2] Serrano JR, Olmeda P, Arnau FJ, Dombrovsky A, Smith L. Turbocharger heat transfer and mechanical losses influence in predicting engines performance by using one-dimensional simulation codes. Energy 2015;86:204–18.

[3] Chesse P, Chalet D, Tauzia X. Impact of the heat transfer on the performance calculations of automotive turbocharger compressor. Oil Gas Sci Technol 2011;66:791–800. https://doi.org/10.2516/ogst/2011129.

[4] Bohn D, Heuer T, Kusterer K. Conjugate flow and heat transfer investigation of a turbo charger. J Eng Gas Turbines Power 2005;127:663–9.

[5] Olmeda P, Dolz V, Arnau FJ, Reyes-Belmonte MA. Determination of heat flows inside turbochargers by means of a one dimensional lumped model. Math Comput Model 2013;57:1847–52.

[6] Romagnoli A, Martinez-Botas R. Heat transfer analysis in a turbocharger turbine: An experimental and computational evaluation. Appl Therm Eng 2012;38:58–77.

[7] Serrano JR, Olmeda P, Arnau FJ, Dombrovsky A, Smith L. Methodology to characterize heat transfer phenomena in small automotive turbochargers: Experiments and modelling based analysis. Proc. ASME Turbo Expo, vol. 1B, 2014. https://doi.org/10.1115/GT2014-25179.

[8] Serrano JR, Olmeda P, Arnau FJ, Samala V. A holistic methodology to correct heat transfer and bearing friction losses from hot turbocharger maps in order to

630 obtain adiabatic efficiency of the turbomachinery. Int J Engine Res
631 2019:1468087419834194. https://doi.org/10.1177/1468087419834194.
632 [9] Tanda G, Marelli S, Marmorato G, Capobianco M. An experimental investigation
633 of internal heat transfer in an automotive turbocharger compressor. Appl Energy
634 2017;193:531–9. https://doi.org/10.1016/j.apenergy.2017.02.053.
635 [10] Baines N, Wygant KD, Dris A. The analysis of heat transfer in automotive
636 turbochargers. J Eng Gas Turbines Power 2010;132:42301.
637 https://doi.org/10.1115/1.3204586.
638 [11] Marelli S, Marmorato G, Capobianco M. Evaluation of heat transfer effects in
639 small turbochargers by theoretical model and its experimental validation. Energy
640 2016;112:264–72. https://doi.org/10.1016/j.energy.2016.06.067.
641 [12] Serrano JR, Olmeda P, Arnau FJ, Reyes-Belmonte MA, Tartoussi H. A study on
642 the internal convection in small turbochargers. Proposal of heat transfer convective
643 coefficients. Appl Therm Eng 2015;89:587–99.
644 [13] Sirakov B, Casey M. Evaluation of Heat Transfer Effects on Turbocharger
645 Performance. J Turbomach 2012;135:21011. https://doi.org/10.1115/1.4006608.
646 [14] Savic B, Gao X, Baar R. Turbocharger Heat Transfer Determination With a
647 Power-Based Phenomenological Approach and a Conjugate Heat Transfer
648 Validation. J Turbomach 2019;141.
649 [15] Gao X, Savic B, Baar R. A numerical procedure to model heat transfer in radial
650 turbines for automotive engines. Appl Therm Eng 2019;153:678–91.
651 [16] Casey M V., Fesich TM. The efficiency of turbocharger compressors with diabatic
652 flows. J Eng Gas Turbines Power 2010;132. https://doi.org/10.1115/1.4000300.

[17] Cormerais M, Chesse P, Hetet JF. Turbocharger heat transfer modeling under steady and transient conditions. Int J Thermodyn 2009;12:193–202. https://doi.org/10.5541/ijot.1034000257.

[18] Marelli S, Gandolfi S, Capobianco M. Heat Transfer Effect on Performance Map of a Turbocharger Turbine for Automotive Application. vol. 2017-March. 2017. https://doi.org/10.4271/2017-01-1036.

[19] Marelli S, Marmorato G, Capobianco M, Rinaldi A. Heat transfer effects on performance map of a turbocharger compressor for automotive application. 2015.

[20] Jiaqiang E, Zhang Z, Tu Z, Zuo W, Hu W, Han D, et al. Effect analysis on flow and boiling heat transfer performance of cooling water-jacket of bearing in the gasoline engine turbocharger. Appl Therm Eng 2018;130:754–66.

[21] Sanguinetti T, Thomas V, Chesse P, Perrot N, Talon V. Implementation of heat transfers in turbocharger models in a system simulation context. Inst. Mech. Eng. - 13th Int. Conf. Turbochargers Turbocharging 2018, 2018, p. 273–87.

[22] Goumy G, Marty P, Chesse P, Perrot N, Dubouil R, Salameh G. Turbocharger Thermal Transfer Model Initialization: Quasi-Adiabatic Map Calculation. 2019. https://doi.org/10.4271/2019-24-0232.

[23] Salameh G, Chesse P, Chalet D, Talon V. Experimental Study of Automotive Turbocharger Turbine Performance Maps Extrapolation. SAE Tech. Pap., vol. 2016- April, 2016. https://doi.org/10.4271/2016-01-1034.

[24] Salameh G, Chesse P, Chalet D. Different Measurement Techniques for Wider Small Radial Turbine Performance Maps. Exp Tech 2016;40:1511–25. https://doi.org/10.1007/s40799-016-0107-8.

676 [25] Salameh G. experimental characterization of an automotive turbocharger turbine
677 and modeling of its performance maps. Ecole Centrale de Nantes (ECN), 2016.
678 [26] Payri F, Olmeda P, Arnau FJ, Dombrovsky A, Smith L. External heat losses in
679 small turbochargers: Model and experiments. Energy 2014;71:534–46.
680 https://doi.org/10.1016/j.energy.2014.04.096.
681 [27] Bergman TL, Incropera FP, DeWitt DP, Lavine AS. Fundamentals of heat and
682 mass transfer. John Wiley & Sons; 2011.
683 [28] Ma Y, He Z, Peng X, Xing Z. Experimental investigation of the discharge valve
684 dynamics in a reciprocating compressor for trans-critical CO2 refrigeration cycle.
685 vol. 32. John Wiley & Sons; 2012.
686 https://doi.org/10.1016/j.applthermaleng.2011.03.022.
687 [29] Perrot N, Chesse P, Dubouil R, Goumy G. Experimental Characterization for
688 Modelling of Turbocharger Friction Losses. vol. 2017-Septe. 2017.
689 https://doi.org/10.4271/2017-24-0013.
690 [30] Deligant M. Caractérisation Numérique et Expérimentale des Performances d'un
691 Turbocompresseur Automobile aux Bas Régimes de Rotation. Paris 6, 2011.
692

693 **FIGURE CAPTIONS LIST**

744